JACS
JOURNAL OF THE AMERICAN CHEMICAL SOCIETY

ARTICLE

pubs.acs.org/JACS

A Triad Interaction in the Fingers Subdomain of DNA Polymerase Beta Controls Polymerase Activity

Drew L. Murphy,[†] Joachim Jaeger,[‡] and Joann B. Sweasy*[,†]

[†]Department of Therapeutic Radiology and Department of Genetics, Yale University School of Medicine, New Haven, Connecticut 06520, United States

[‡]Wadsworth Center, New York State Department of Health, Center for Medical Science, 150 New Scotland Avenue, Albany, New York 12208, United States

Supporting Information

ABSTRACT: DNA polymerase beta (pol beta) is the main polymerase involved in the base excision repair pathway responsible for repairing damaged bases in the DNA. Previous studies on the H285D mutant of pol beta suggested that the C-terminal region of the polymerase is important for polymerase function. In this study, the C-terminal region of pol beta was mutated to assess its role in polymerization. Kinetic experiments showed that the C-terminal region is required for wild-type polymerase activity. Additionally, an interaction between the fingers and palm subdomain revealed itself to be required for polymerase activity. The E316R mutant of pol beta was shown to have a 29 000-fold reduction in polymerization rate with no reduction in nucleotide binding, suggesting that there exists a noncovalent mechanistic step between nucleotide binding and nucleophilic attack of the primer 3′-hydroxyl group on the α-PO_4 of the nucleotide. Molecular modeling studies of the E316R mutant demonstrate that disrupting the interaction between Arg182 and Glu316 disrupts the packing of side chains in the hydrophobic hinge region and may be hampering the conformational change during polymerization. Taken together, these data demonstrate that the triad interaction of Arg182, Glu316, and Arg333 is crucial for polymerase function.

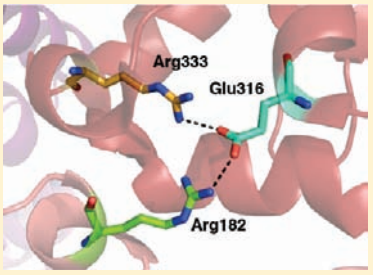

INTRODUCTION

Endogenous cellular DNA damage occurs at a rate of at least 20 000 lesions per cell per day.[1] These endogenous lesions are repaired by the base excision repair (BER) machinery, and correct repair of these lesions is critical for genome stability. DNA polymerase beta (pol beta) is a key enzyme in the BER pathway, which along with its polymerase activity also possesses 5′-deoxyribose phosphate (dRP) lyase activity.[2] The polymerase contains four subdomains: the 8kD domain houses the dRP lyase activity, the thumb subdomain is critical for DNA binding, the palm subdomain contains the active site residues required for polymerization, and the fingers domain is largely responsible for nucleotide binding (Figure 1). Unlike other eukaryotic polymerases such as pol δ and pol ε,[3] pol beta does not possess any proofreading exonuclease activity, although AP Endonuclease 1 (APE1) may function as a proofreading exonuclease for pol beta.[4] A relatively error-prone polymerase, pol beta inserts an incorrect nucleotide in approximately one out of every 10 000 nucleotides.[5] These errors in DNA repair can increase genomic instability if carried through further cell divisions. An increase in genomic instability has been shown to lead to the generation of a mutator phenotype, which in turn can produce a malignant phenotype.[6] Pol beta functions both in BER and in meiosis[7] and, additionally, pol beta variants have been found in a wide range of cancerous tissue.[5] Therefore, studying pol beta and its variants can lead to a deeper understanding of the mechanistic basis of cancer.[8]

Earlier studies of an AZT-resistant variant of pol beta, H285D,[9] found this mutation to be subtly mutagenic. The H285D pol beta mutant is capable of extending mispaired primer termini in gapped DNA. This is accomplished through a tighter binding of the incoming nucleotide in the mutant as compared to wild-type pol beta. Computer modeling studies of Asp285 pol beta showed that the negatively charged Asp285 side chain is closer to the positively charged Lys289 side chain as compared to wild-type pol beta. This ablates the interaction that both Lys289 and His285 have with the backbone carbonyl oxygen of Ile323, which allows for the C-terminal tail of pol beta (327−335) to move farther away from helix N. In turn, it was postulated that loss of this His285/Ile323/Lys289 "anchor" would allow for the C-terminal residues of pol beta to be more mobile, which could, due to the closeness of the C-terminus to the active site, alter nucleotide binding.

In this study, the C-terminal region of pol beta was examined in further depth. It was found that the C-terminal residues of pol beta are required for wild-type activity of the polymerase. A key residue in the C-terminal region (Arg333) was shown to be required for pol beta activity, and this residue interacts with a glutamate side chain in the fingers subdomain (Glu316). This interaction was determined to be necessary for proper pol beta function by kinetic analysis of a number of polymerase mutants,

Received: December 9, 2010
Published: March 31, 2011

dx.doi.org/10.1021/ja111099b | J. Am. Chem. Soc. 2011, 133, 6279–6287

where every substitution made at either Arg333 or Glu316 obliterated pol beta activity. Glu316 also interacts with Arg182 in the palm subdomain. Arg182 is adjacent to Arg183, which binds to a nonbridging oxygen on the β-phosphate of the incoming nucleotide. Mutants of Arg182 also exhibit dramatically reduced polymerase activity, indicating that all three residues are instrumental for proper pol beta function. Further analysis indicated that Arg182, Glu316, and Arg333 greatly affect the activity of the polymerase with only subtle effects seen in the binding of nucleotide. It is suggested that the interactions between these three residues are important for the dynamics of the polymerase and that mutants of these residues may be affecting noncovalent steps during catalysis.

MATERIALS AND METHODS

Expression and Purification of Pol Beta Proteins. The wild-type pol beta cDNA was cloned into the pET28a vector as previously described.[9] All the mutations were introduced into the wild-type pol beta plasmid using the QuickChange site-directed mutagenesis protocol (Stratagene) with DNA oligonucleotide primers (Invitrogen, Table S1). The presence of the mutations was confirmed by sequence analysis (Keck DNA Sequencing Facility, Yale University School of Medicine).

Wild-type and mutant pol beta pET28a plasmids were transformed into *E. coli* (BL21 DE3). Luria Broth cultures (500 mL) were inoculated with a 5 mL overnight starter culture and incubated at 37 °C until the $OD_{600\ nm}$ reached approximately 0.6. Isopropyl β-D-thioaglactopyranoside (IPTG) was added to a final concentration of 1 mM and incubated at 30 °C for 4 h to induce expression of pol beta. After induction, the bacteria were pelleted and stored at 4 °C on ice overnight. The cells were resuspended in buffer B (40 mM Tris-HCl pH 8, 500 mM NaCl, 5 mM imidazole) with added protease inhibitors (Roche) and 1 mM PMSF and lysed by sonication. The lysate was clarified by centrifugation, and pol beta was purified by fast protein liquid chromatography. First, a 5 mL HiTrap Chelating HP Column (GE Healthcare) charged with $NiSO_4$ was employed using a linear gradient from 5 to 500 mM imidazole in buffer B. Pol beta eluted from this column in a broad peak from 208 to 248 mM imidazole. Pol beta fractions were combined, concentrated to ~1 mL, and diluted to 10 mL in buffer D (50 mM Tris-HCl pH 8, 100 mM NaCl, 1 mM EDTA, 10% glycerol). This solution was then applied to a 5 mL HiTrap SP HP column (GE Healthcare), and a linear gradient from 100 to 2000 mM NaCl was employed. Pol beta eluted in a sharp peak at 1100 mM NaCl. Pol beta containing fractions were combined, concentrated to ~500−700 μL, and glycerol was added to a final concentration of 15%. The final protein, which was >90% pure by SDS-PAGE gel analysis, was aliquoted, flash frozen in liquid nitrogen, and stored at −80 °C. Final protein concentration was determined using the absorbance at 280 nm and the extinction coefficient for pol beta (ε = 21 200 M^{-1} cm^{-1}).

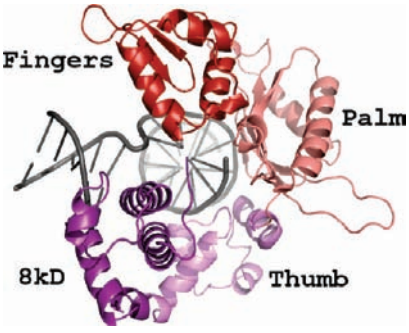

Figure 1. DNA polymerase beta contains four subdomains: 8kD, thumb, palm, and fingers. A cartoon representation of the binary complex (1bpx) of pol beta (color) and 1bp-gap DNA (gray).

DNA Substrate for Biochemical Assays. DNA oligos were purchased from the Keck Oligo Synthesis Resource (Yale University, Table 1) and purified by polyacrylamide gel electrophoresis prior to use. The 5′ end of the primer strand (U22, Table 1) was labeled with ^{32}P, the downstream oligo (D22, Table 1) was phosphorylated on the 5′ end, and the three oligos were annealed to generate the 1bp-gap DNA substrate, as described previously.[9]

Presteady-State Kinetic Analysis. Rapid chemical quench kinetics were performed using the KinTek Chemical Quench-Flow (RQF-3) apparatus.[10] Single-base gapped DNA substrate (Table 1) with a template A at the gap was used. Two 2× reaction mixtures (600 nM DNA + 200 nM pol beta and 200 μM dTTP + 20 mM $MgCl_2$) in reaction buffer (50 mM Tris-Cl pH 8, 20 mM NaCl, 6 mM DTT, 10% glycerol) were combined (15 μL each) in the apparatus, rapidly mixed, quenched with 0.5 M EDTA, and combined with 50 μL of 90% formamide dye. A time course of reactions from 0.02 to 3.0 s (or 0.5−60 s) was conducted. Final reaction concentrations were 300 nM DNA, 100 nM pol beta, 100 μM dTTP, and 10 mM $MgCl_2$ in reaction buffer. Completed reactions were separated using denaturing 20% polyacrylamide gel electrophoresis and visualized and quantified using a Storm 860 phosphorimager with ImageQuant software. Kinetic data were plotted and fit using KaleidaGraph software (Synergy software) to the biphasic burst equation:

$$[\text{product}] = [\text{E}]_{\text{app}}\left[\frac{(k_{\text{obs}})^2}{(k_{\text{obs}}+k_{\text{ss}})}x(1-\text{e}^{-(k_{\text{obs}}+k_{\text{ss}})t}) + \left(\frac{k_{\text{obs}}k_{\text{ss}}}{(k_{\text{obs}}+k_{\text{ss}})}t\right)\right]$$

or to a single exponential equation:

$$[\text{product}] = A(1-\text{e}^{-k_{\text{obs}}t})$$

where A is the amplitude, k_{obs} is the observed rate constant of the exponential phase, and k_{ss} is the rate constant for the linear (or steady-state) phase.[11]

Some mutants produced little to no extended DNA product within the time frame of the KinTek apparatus. In this case, the presteady-state kinetics experiments were conducted manually using the above reaction conditions with longer time courses ranging from 20 s to 60 min.

Table 1. DNA Oligonucleotides and 1bp-Gap DNA Substrate Used in This Study[a]

oligonucleotide	DNA sequence (5′ to 3′)
U22	GCCTCGCAGCCGTCCAACCAAC
D22	CAACCTCGATCCAATGCCGTCC
45AG	GGACGGCATTGGATCGAGGTTG**A**GTTGGTTGGACGGCTGCGAGGC
1 bp-gap DNA (U22 + D22 + 45AG)	5′ GCCTCGCAGCCGTCCAACCAAC CAACCTCGATCCAATGCCGTCC
	3′ CGGAGCGTCGGCAGGTTGGTTG**A**GTTGGAGCTAGGTTACGGCAGG

[a] Templating base is bold and underlined.

dx.doi.org/10.1021/ja111099b | J. Am. Chem. Soc. 2011, 133, 6279–6287

Scheme 1. The Mechanism of Polymerization by DNA Polymerase Beta

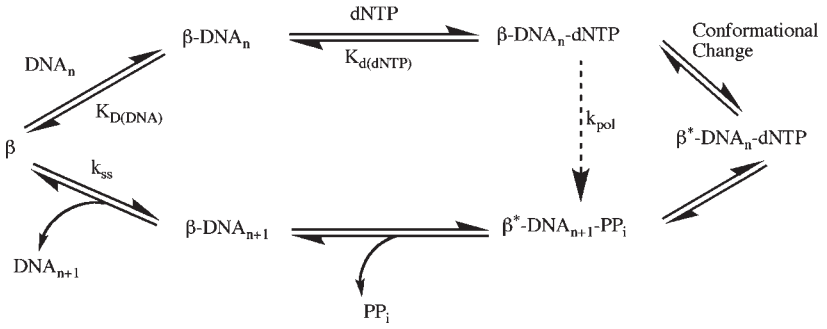

Reaction products were analyzed and fit to the single exponential equation, as above.

Circular Dichroism Spectroscopy. Circular dichroism spectra were collected for each pol beta protein using a Chirascan circular dichroism spectrometer (Applied Photophysics). Ellipticity of a 1 μM solution of pol beta in 10 mM K_2HPO_4 at 23 °C was measured from 280 to 190 nm.

Single Turnover Kinetics. To assess the mechanism of polymerization of the charge reversal mutants in greater detail, single turnover kinetics was employed. Single turnover kinetics allows for the determination of both the maximum rate of polymerization (k_{pol}) and the dissociation constant for the incoming nucleotide ($K_{d(dNTP)}$).

For nucleotide incorporation with wild-type pol beta, a mixture of 500 nM active pol beta (active site titration; K. Donigan unpublished result) and 50 nM 1bp-gap DNA (final concentrations) was reacted with varying concentrations of dTTP (1−200 μM) and 10 mM $MgCl_2$ (final concentrations) in reaction buffer. A separate time course from 0.03 to 10 s was conducted for each concentration of dTTP using the KinTek apparatus. Reactions were analyzed as above, and kinetic data were fit to the single exponential equation:

$$[\text{product}] = A(1 - e^{-k_{obs}t})$$

where A is the amplitude, k_{obs} is the observed rate constant, and t is the time. A secondary kinetic plot was constructed by plotting the observed rate constant (k_{obs}) versus [dTTP], which was then fitted to the hyperbolic equation:

$$k_{obs} = \frac{k_{pol}[\text{dTTP}]}{K_{d(\text{dTTP})} + [\text{dTTP}]}$$

where k_{pol} is the maximum rate of polymerization and $K_{d(dNTP)}$ is the equilibrium dissociation constant of dNTP.

Single turnover kinetics of the mutants were examined in a similar fashion, with some changes. For R333E and R333Stop, 500nM pol beta and 50 nM 1bp-gap DNA were reacted in the KinTek apparatus as described above, except higher concentrations of dTTP were used (10−600 μM) for longer time frames (1−60 or 180 s). The R182E and E316R experiments were conducted manually under similar conditions using 5−1000 μM dTTP and time courses from 15 s to 60 min. In all of the mutant cases, the polymerase-to-DNA ratio allowed for at least 93% of the DNA to be bound by pol beta, based on the $K_{D(DNA)}$ from gel mobility shift experiments (data not shown).

Molecular Modeling and Molecular Dynamics Simulations. Models of the E316R, R333E, and E316R/R333E mutants of pol beta were generated using a high-resolution DNA cocrystal structure (PDB code 2fms). The overall root-mean-square deviation of this structure from ideal bond lengths is 0.005 Å at a free R-factor of 0.244. The experimental coordinate error of this well-refined starting model is about 0.2 Å, and thus the overall structure was always well behaved during modeling, minimization, and equilibration phase of the simulations. The amino acid substitutions are located at the surface of the fingers domain and modeled using the programs PyMol and VMD.[12] Initial close contacts were carefully analyzed in PyMol and removed by selecting frequently found side chain rotamers that as much as possible resembled conformations found in the parent structure. The CHARMM27 force field was used to parametrize atomic interactions with short-range nonbonding terms calculated up to a 12 Å cutoff for electrostatic and van der Waals interactions. Contributions from long-range interactions were considered using the particle-mesh-Ewald scheme implemented in NAMD2 version 2.7.[13] All hydrogen-bond lengths were held constant with the SHAKE-RATTLE-ROLL algorithm. The TIP3P model was applied for description of the water molecules surrounding the protein. The ionic strength was adjusted to 0.2 mol/L for more appropriate screening of Coulomb forces. The PyMol optimized models were subjected to 10 000 steps of energy minimzaion followed by 1 ps of a periodic-boundary equilibration molecular dynamcis simulation with a time step of 1 fs using the NAMD2 simulation package version 2.7.[13] This protocol was then followed by a 5 ns production MD simulation where the simulation temperature was also maintained at 310 K using a temperature bath with a coupling constant of 5 ps^{-1}. Root-mean-square deviation analyses were performed to evaluate systems mobility and proper convergence (data not shown). Trajectory analysis and molecular graphics images were generated using VMD and PyMol.

RESULTS

To explore the role of the C-terminal residues in the function of DNA polymerase beta (pol beta), a series of truncation mutants of pol beta were generated. Truncations at the C-terminus were constructed by introducing a stop codon at positions 1, 2, 3, 6, and 9 residues from the wild-type stop codon position: E335Stop, S334Stop, R333Stop, P330Stop, and Y327Stop, respectively. Once the requirement for Arg333 and its interaction with Glu316 were realized, this interaction was probed using three types of mutants. First, substitutions of Arg333 and Glu316 were made with glycine, and hydrophobic residues of similar size were made to examine the requirement for side chains and charges, respectively (E316G, E316I, R333G, and R333M). Next, residues of opposite charges were substituted at positions 316 and 333, to determine if the specific charges of glutamate and arginine are required (E316K, E316H, E316R, R333D, and R333E). Finally, conservative substitutions where Arg333 and Glu316 were replaced with an amino acid with the same charge were constructed (E316D, R333H, and R333K). The pol beta double mutant, E316R/R333E, was made to examine the

dx.doi.org/10.1021/ja111099b | J. Am. Chem. Soc. 2011, 133, 6279–6287

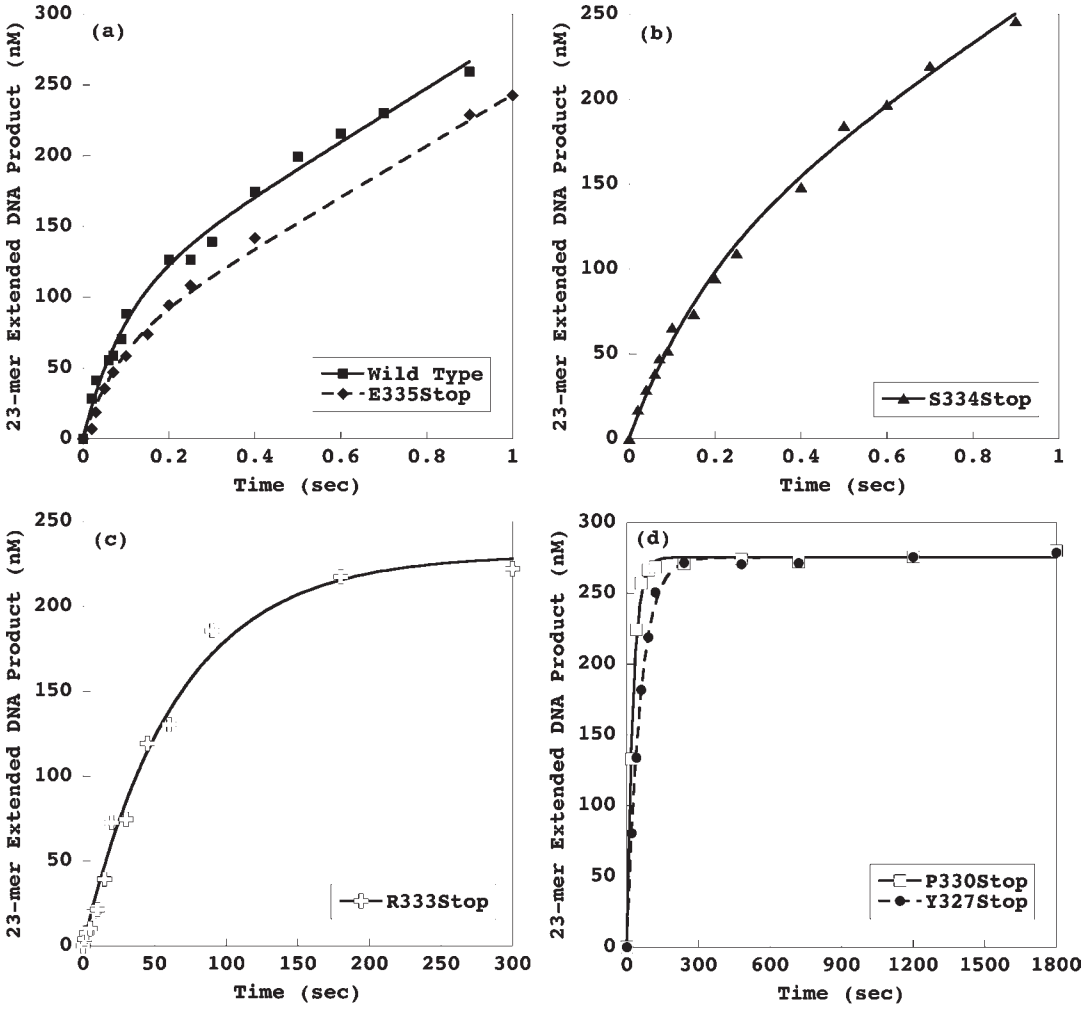

Figure 2. Representative presteady-state plots of wild-type pol beta and truncated mutants. (a and b) Wild type, E335Stop, and S334Stop exhibit fast biphasic burst kinetics (k_{obs} = 9 ± 2, 9 ± 1, 5 ± 1 s^{-1} and k_{ss} = 3 ± 1, 2.4 ± 0.6, and 1.5 ± 0.2 s^{-1}, respectively). (c and d) R333Stop, P330Stop, and Y327Stop are much slower with rates 270- and 530-fold slower than wild type.

Table 2. Polymerization Rate Varies with the Length of the Tail[a]

	tail sequence	k_{obs} (s^{-1})	fold change (wild type/mutant)
wild type	...KYREPKDRSE	9 ± 2	1
E335Stop	...KYREPKDRS	9 ± 1	1
S334Stop	...KYREPKDR	5 ± 1	2
R333Stop	...KYREPKD	0.017 ± 0.003	530
P330Stop	...KYRE	0.038 ± 0.002	270
Y327Stop	...K	0.026 ± 0.009	350

[a] Presteady-state rates were measured as described in the Materials and Methods for the truncated pol beta mutants. E335Stop and S334Stop are fast and exhibit biphasic burst kinetics, while the shorter truncations of R333Stop, P330Stop, and Y327Stop are 270−530 times slower than wild type. Data shown are the average of several experiments with standard deviation.

reversibility of this interaction. Finally, once Arg182 was identified as a player in a triad interaction with Arg333 and Glu316, all of the same types of substitutions were made at position 182 (R182G, R182M, R182E, and R182K).

Polymerization Rate Varies with Tail Length. The mechanism of DNA polymerase beta (Scheme 1) consists of four main steps: DNA binding, dNTP binding, chemistry, and product release. First, DNA is bound by pol beta with a characteristic equilibrium dissociation constant ($K_{D(DNA)}$), producing the binary polymerase−DNA complex (Figure 1). The binary complex then binds nucleotide (dNTP). Nucleotide binding initiates the conformational change in the polymerase, which moves the fingers domain and the 8kD domain closer together, essentially closing the polymerase around the dNTP. Closing of the polymerase induces chemistry at a rate of k_{pol}. Upon addition of the nucleotide to the DNA, the polymerase reopens and releases the extended DNA product, which is the overall rate-limiting step in this cycle. Wild-type pol beta exhibits typical biphasic burst kinetics with a burst rate of 9 s^{-1}, as shown in Figure 2a, which is consistent with previously reported values.[14] The biphasic burst is indicative of the polymerization mechanism of pol beta wherein there is a rapid, first-order step followed by a slower, zero order, rate-limiting product release step. Like the wild-type pol beta, E335Stop and S334Stop also exhibit biphasic burst kinetics (k_{obs} = 9 and 5 s^{-1}, respectively, Figure 2 and Table 2). The shorter truncations of R333Stop, P330Stop, and Y327Stop are 270−530 times slower

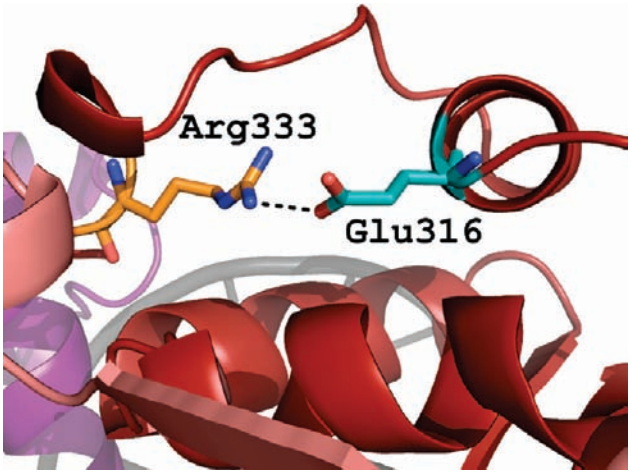

Figure 3. Glu316 interacts with Arg333. In both the closed (1bpy; pictured) and the open (1bpx) crystal structure of wild-type pol beta, Arg333 (orange) interacts with Glu316 (cyan): 2.7 Å (1bpy), 3.1 Å (1bpx). This interaction could be the key to the requirement for Arg333 on wild-type pol beta activity.

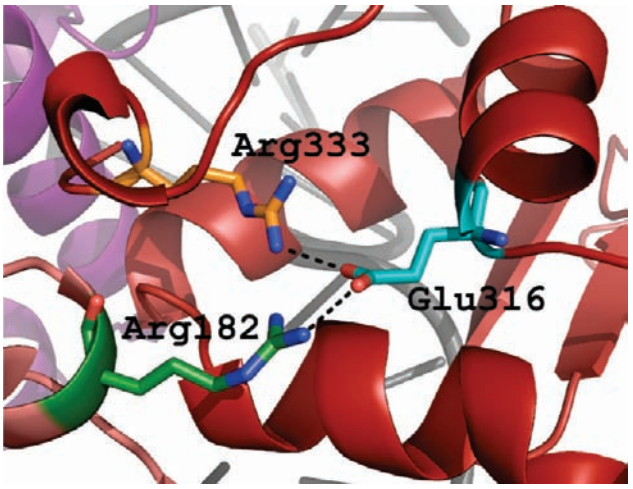

Figure 4. Glu316 interacts with Arg333 and Arg182. Glu316 (cyan) possesses close contacts with both Arg333 (orange; 2.7 Å (1bpy), 3.1 Å (1bpx)) and Arg182 (green) in both the closed (1bpy; pictured, 3.0 Å) and the open (1bpx, 2.9 Å) crystal structures of pol beta.

Table 3. Presteady-State Rates for Mutants at Residues 316 and 333[a]

mutant	316	333	k_{obs} (s^{-1})	fold change (wild type/mutant)
wild type	Glu	Arg	9 ± 2	1
E316G	Gly	Arg	0.024 ± 0.002	380
R333G	Glu	Gly	0.047 ± 0.004	190
E316I	Ile	Arg	0.0102 ± 0.0008	880
R333M	Glu	Met	0.087 ± 0.008	100
E316K	Lys	Arg	0.00067 ± 0.00005	13 000
E316R	Arg	Arg	0.0011 ± 0.0002	8000
E316H	His	Arg	0.011 ± 0.005	800
R333D	Glu	Asp	0.023 ± 0.0002	390
R333E	Glu	Glu	0.0018 ± 0.0003	5000
E316D	Asp	Arg	0.060 ± 0.006	150
R333K	Glu	Lys	0.025 ± 0.0004	360
R333H	Glu	His	0.024 ± 0.0003	380
E316R/R333E	Arg	Glu	0.00065 ± 0.00009	14 000

[a] Any alteration of either Arg333 or Glu316 obliterates wild-type pol beta activity.

Table 4. Presteady-State Rates for Mutants Arg182[a]

mutant	k_{obs} (s^{-1})	fold change (wild type/mutant)
wild type	9 ± 2	1
R182K	0.26 ± 0.03	35
R182M	0.065 ± 0.010	140
R182G	0.053 ± 0.010	170
R182E	0.0088 ± 0.0004	1000

[a] Any alteration of either Arg182 drastically reduces polymerase activity.

than wild type, as shown in Figure 2c and d and Table 2. Additionally, the kinetics are no longer biphasic but rather fit to a single exponential, indicating that a step before chemistry or chemistry itself has now overtaken product release as the rate-limiting step in the polymerization cycle for these mutants. The stark difference in the reaction rates between S334Stop and R333Stop suggests that Arg333 is critical for normal pol beta activity.

Pol Beta Truncations and Substitutions Do Not Drastically Alter the Polymerase's Global Structure. To assess the overall folding and stability of the mutant polymerases, circular dichroism spectroscopy was employed. All truncated mutants of pol beta exhibit a similar circular dichroism spectrum as the wild-type protein (Figure S1). This indicates that the final C-terminal nine amino acid residues are not required for overall wild-type-like structure and that deleting these residues does not grossly alter the folding of pol beta. Additionally, all amino acid substitutions do not alter the overall total folding of pol beta. Circular dichroism spectra of each substitution mutant and the E316R/R333E double mutant are indistinguishable from that of the wild-type polymerase (data not shown).

Arg333 Interacts with Glu316. In both the ternary (1bpy; Figure 3) and the binary (1bpx) crystal structures of wild-type pol beta, Arg333 interacts with Glu316 (2.7 Å, 1bpy; 3.1 Å, 1bpx). This interaction could be the key to the requirement for Arg333 on wild-type pol beta activity. To examine the involvement of this interaction on pol beta activity, mutants of each residue were constructed as described above. Glycine and hydrophobic mutants of residues 333 and 316 exhibit 100−880-fold reduced activity as compared to wild-type pol beta, as shown in Table 3. Together, these results show that residues 333 and 316 cannot be hydrophobic for proper pol beta function. When Arg333 and Glu316 were substituted with residues of opposite charge, the polymerization rate is dramatically decreased, 390−13 000-fold (Table 3). Therefore, residues 333 and 316 having the same charge as one another is extremely detrimental to polymerase activity. Finally, conservative substitutions were made at residues 333 and 316. Strikingly, these pol beta mutants were as impaired as the previous mutants (150−380-fold decrease vs wild type; Table 3). Thus, any alteration of either Arg333 or Glu316 obliterates wild-type pol beta activity. This indicates that not only is Arg333 crucial for polymerase activity, but the interaction between Arg333 and Glu316 is absolutely required for normal pol beta function.

dx.doi.org/10.1021/ja111099b | J. Am. Chem. Soc. 2011, 133, 6279–6287

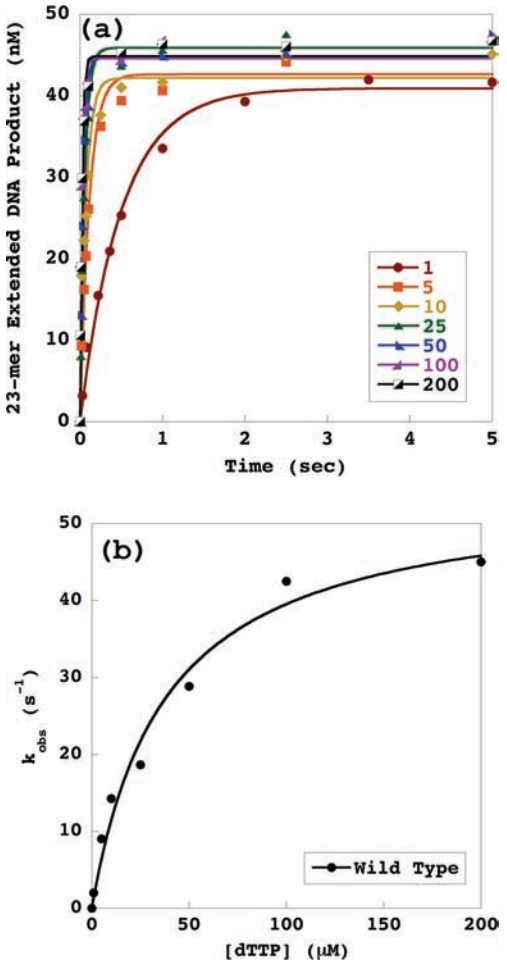

Figure 5. Wild-type pol beta exhibits fast polymerization and tight dNTP binding under single turnover conditions. Representative single turnover plots of (a) extended product versus time from which the observed rate constants (k_{obs}) for each dTTP concentration were calculated and of (b) k_{obs} versus the concentration of dTTP for wild-type pol beta, from which the maximum rate of polymerization (k_{pol}) and equilibrium dissociation constant for dTTP ($K_{d(dTTP)}$) were calculated, as described in the Materials and Methods.

The Arg333−Glu316 Interaction Is Not Reversible. In an attempt to recapitulate the activity of wild-type pol beta, the E316R/R333E double mutant was constructed. This mutant possesses the same amino acid side chains as the wild-type polymerase but in the opposite orientation; however, this double mutant does not retain the wild-type pol beta activity. Interestingly, the double mutant is one of the slowest of the mutants observed in this study and is 14 000-fold slower than wild type (0.00065 s^{-1}, Table 3). Clearly, the exact identities and spatial juxtaposition of both Arg333 and Glu316 are absolutely required for wild-type activity of pol beta.

Arg182 Is Required for Wild-Type Pol Beta Activity. Closer examination of the crystal structure revealed that Glu316 interacts not only with Arg333 but with Arg182 as well (Figure 4). Glu316 makes close contacts with both Arg333 and Arg182 in both the open and the closed (pictured, Figure 4) crystal structures of pol beta. Arg182 is adjacent to Arg183, which directly binds a nonbridging oxygen in the β-phosphate group of the dNTP. This contributes to proper geometric alignment of all atoms in the active site that are involved in the catalytic step (Mg, α-phosphate, 3′-OH on primer terminus).

Any mutation of Arg182 drastically reduces pol beta activity, as shown in Table 4. Arg182 was mutated to Lys, Met, Gly, and Glu. As was the case with Arg333 and Glu316, all substitutions of residue 182 resulted in a polymerase with a dramatically reduced rate (35−1000-fold vs wild type; Table 4) Thus, not only is a charged residue at this position required, the charge must be positive and the residue needs to be an arginine side chain to realize full wild-type pol beta activity. This demonstrates that Arg182 is crucial for the activity of pol beta.

The Interactions between Arg333, Glu316, and Arg182 Are Important for Catalysis by Pol Beta. Single turnover kinetics was used to examine the R333E, E316R, R182E, and R333Stop mutants of pol beta in closer detail. Wild-type pol beta exhibits fast polymerization (54 s^{-1}) and tight dNTP binding (38 μM) under single turnover conditions (Figure 5 and Table 5). As was seen with the presteady-state kinetics, each of these mutants is slower than wild-type pol beta (390−29 000-fold). These results suggest that the chemistry of nucleotide incorporation has been dramatically altered in these mutants. Interestingly, this set of impaired polymerases only exhibits small changes in dNTP binding. The equilibrium dissociation constant for nucleotide is the same as for the wild-type polymerase (0.5−3-fold). This indicates that these mutations are not greatly affecting the dNTP binding pocket in the enzyme. Coupled with the dramatic decrease in polymerization rate, these results suggest that these mutants are impaired either in a mechanistic, likely noncovalent, step that occurs between nucleotide binding and chemistry or in the chemistry itself.

The most striking example in this set of mutants is the E316R pol beta mutant. This mutation has no effect on the binding of nucleotide, yet it reduces the polymerization rate of the enzyme by 29 000-fold (Table 5 and Figure 6).

Substitution of Glutamate at Residue 333 Disrupts the Triad Interaction. Molecular dynamics simulations of the R333E mutant show that the glutamate moves away from the location that used to be occupied by Arg333 in the wild-type structure (Figure 7c). The movement of Glu333 leads to a significant rearrangement in backbone and side chain positions of residues 327, 328, and 329. The structural repositioning of Glu333 in conjunction with the reduced polymerization rate of the Arg333 mutants (Table 3) indicates that the Arg182−Glu316 interaction alone is not sufficient for wild-type polymerase activity. The additional substitution of Arg316 with Glu333 (E316R/R333E) via NAMD2 molecular dynamics shows that Arg182 repositions to interact favorably with Glu333 (Figure 7d). However, Arg316 is spatially and electrostatically constrained by the closing in of Arg182 and the presence of the additional positive charge. The arrangement of side chains in the E316R/R333E double mutant differs considerably from that in the corresponding region of the wild-type structure. Even though there exists a favorable interaction between Arg316 and Glu333, the polymerization rate of the double mutant is dramatically decreased. These data along with the data for the R182E mutant (Table 4) suggest that the interaction between residues 316 and 333 is not sufficient for wild-type polymerase activity. Clearly, an intact triad interaction between Arg182, Glu316, and Arg333 is required for proper polymerase function.

Table 5. Single Turnover Kinetic Data for the Most Damaging Mutants

	k_{pol} (s^{-1})	fold change in k_{pol}[a]	K_d (μM)	fold change in K_d[a]
wild type	54 ± 4	1	38 ± 8	1
R182E	0.034 ± 0.002	1600	131 ± 19	3
E316R	0.00185 ± 0.00006	29 000	20 ± 4	0.5
R333E	0.074 ± 0.003	730	70 ± 9	2
R333Stop	0.139 ± 0.007	390	56 ± 11	1

[a] Fold change expressed as wild type/mutant for k_{pol} and mutant/wild type for K_d.

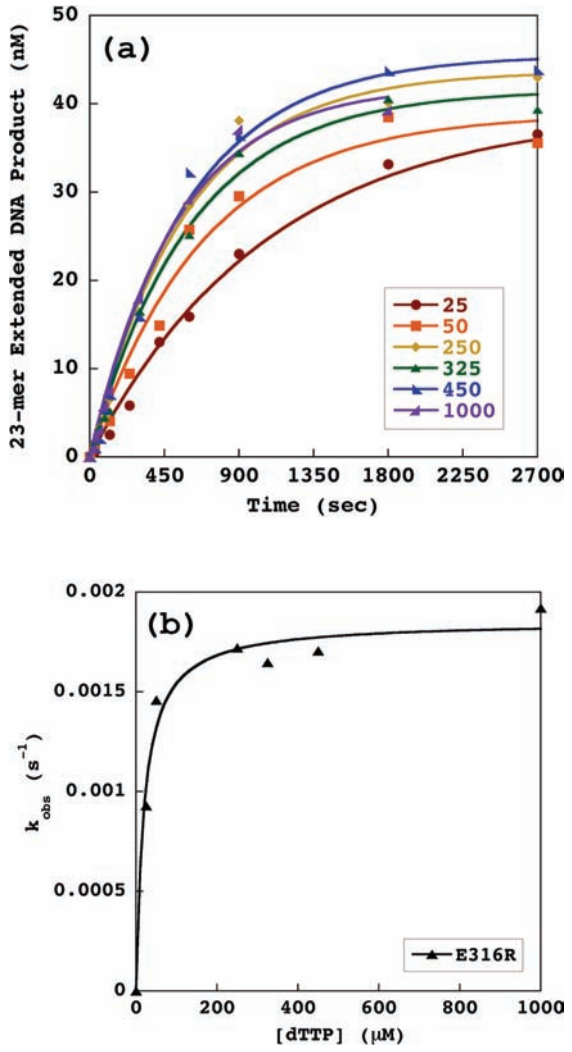

Figure 6. Single turnover plots for the E316R mutant of pol beta. (a) Plot of extended product versus time. (b) Observed rate constants (k_{obs}, calculated from (a)) plotted versus the concentration of dTTP to generate a hyperbolic plot to calculate the maximum rate of polymerization (k_{pol}) and equilibrium dissociation constant for dTTP ($K_{d(dTTP)}$).

Mutation of Glu316 to Arg May Disrupt Proper Function of the Hydrophobic Hinge of Pol Beta. Computer modeling and fully equilibrated, periodic boundary molecular dynamics simulations suggest that mutation of E316R causes repulsion of the charged head groups of Arg182 and Arg316 (Figure 7b). Consequently, the local structure is substantially altered. Upon moving away from Arg182, Arg316 approaches an area occupied by Tyr266, pushing it out of the way (Figures 8 and S2). This change leads to a rearrangement of other hinge residues located in this region, Thr196, and to a lesser extent Ile174 and Tyr265.

The simulation shows additional movements in a loop at positions Gly184 and Ala185, although the interactions between the triphosphate moiety and residues Ser180, Arg183, and Ser273 remain tight throughout the simulation. Surface rendering of the dNTP pocket indicates that the volume of the pocket remains essentially unchanged as compared to wild type. Also, Arg 183 remains in contact with the β-phosphate oxygen during the simulations, thereby corroborating the small changes in dNTP binding constants (Table 5). Maintaining wild-type-like dNTP interactions combined with the dramatic rearrangement of hinge residues on the exterior face of the fingers domain provide important clues as to the kinetic phenotype of these charge reversal mutants.

DISCUSSION

Pol beta is the main polymerase involved in BER and, as such, is responsible for the repair of many DNA lesions. Previous biochemical studies of a subtle mutator mutant of pol beta (H285D)[9] hinted that the C-terminal tail region (residues 327−335) of pol beta may be important for proper function of the polymerase. In this work, the tail region of pol beta was investigated in greater detail, revealing a heretofore unrealized requirement for pol beta polymerase activity. A triad interaction exists in the C-terminal domain of pol beta wherein Glu316 forms close contacts with both Arg182 and Arg333. This triad is located near the surface of the polymerase and is adjacent to the hydrophobic hinge region and is connected directly to the nucleotide binding arena via a helical turn containing Arg183.

The Entire Triad Is Required for Wild-Type Pol Beta Activity. Truncated mutants of pol beta revealed a requirement of Arg333 for pol beta activity, evidenced by the 530-fold drop in polymerization rate between the S334Stop and R333Stop mutants (Figure 2 and Table 2). Examination of the ternary structure of pol beta (dNTP bound; 1bpy) showed that Glu316 is interacting with Arg333. This interaction was examined through extensive mutagenesis experiments. Every mutant of either residue 316 or 333 resulted in near-complete obliteration of the polymerization rate of pol beta (100−13 000-fold; Table 3). Surprisingly, the double mutant, E316R/R333E, which merely reverses the locations of the wild-type residues also had an extraordinarily slow polymerization rate (14 000-fold slower than wild type; Table 3). This result with the double mutant suggested that another player may be involved in this scenario; indeed, Arg182 also interacts with Glu316. Mutants of Arg182 displayed the same reduction in polymerization rate as mutants of Arg333 and Glu316 (35−1000-fold reduction over wild type; Table 4). Also of note, in a computational study, Arg182, Glu316, and Arg333 were implicated in having

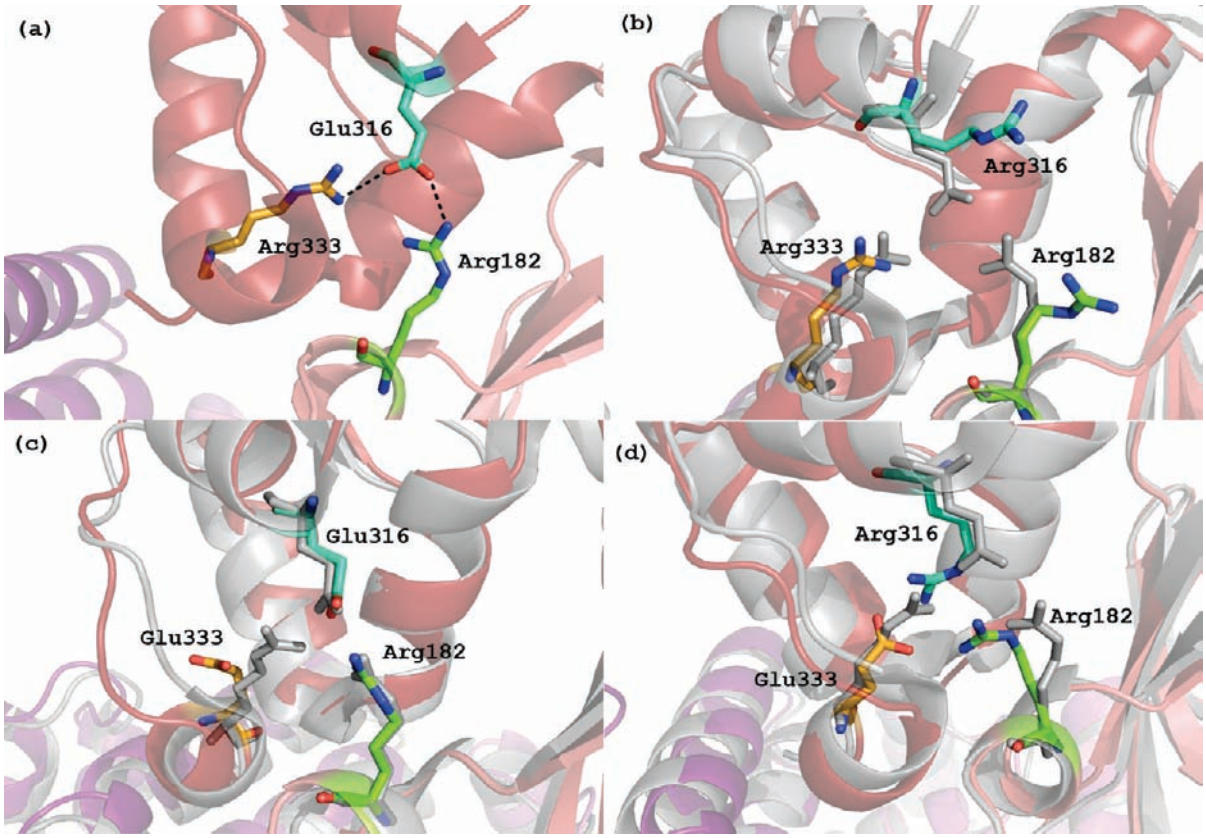

Figure 7. Substitution of Glu316 and/or Arg333 destroys the triad interaction. (a) The wild-type ternary (closed; dNTP bound, 2fms) crystal structure showing the interaction between Arg333, Glu316, and Arg182. Residue 316 and 333 substitutions modeled into pol beta by molecular dynamics simulations and superimposed over the wild-type (2fms) structure, shown in gray: (b) Arg316, (c) Glu333, and (d) Arg316 and Glu333.

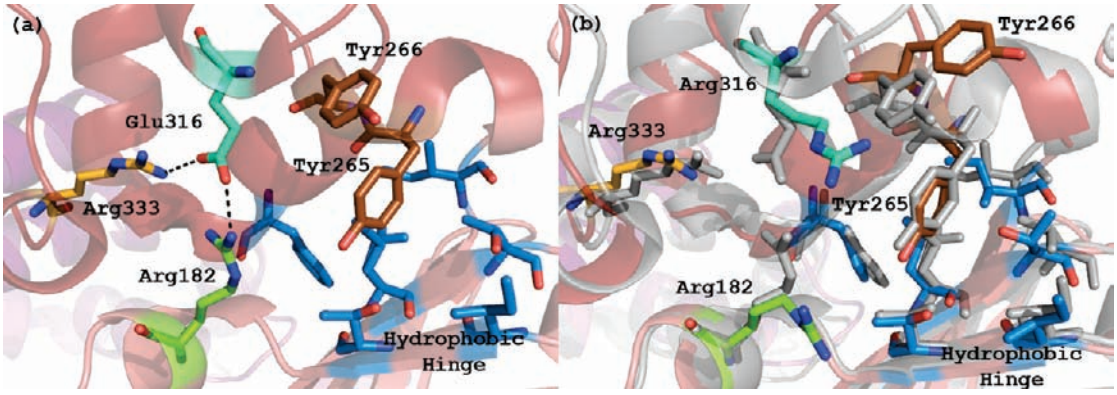

Figure 8. Repulsion between Arg182 and Arg316 disrupts the hydrophobic hinge. (a) The wild-type ternary (closed; dNTP bound, 2fms) crystal structure showing the triad interaction, the hydrophobic hinge (Ile174, Thr176, Leu194, Thr196, Ile260, and Phe272), and Tyrs 265 and 266. (b) Molecular dynamics simulations of Arg316 substitution superimposed over the wild-type (2fms) structure shown in gray.

electrostatic contributions to the stabilization of the transition state during the nucleophilic addition of nucleotide to the primer strand.[15] Any mutation made at these positions in the polymerase, including the conservative mutations (R182K, E316D, and R333K), drastically reduced the polymerization rate, thus indicating that the entire triad as it is found in the wild-type pol beta is required for full polymerase activity.

To tease out mechanistic details of how this triad interaction is involved in polymerization, single turnover kinetic experiments were performed on the most damaging of this set of mutants: R182E, E316R, R333E, and R333Stop. These results show that again the polymerization rate (k_{pol}) is drastically reduced (390−29 000-fold vs wild type; Table 5). Strikingly, the equilibrium dissociation constants for nucleotide ($K_{d(dNTP)}$) are similar to that of wild type (0.5−3-fold; Table 5). The E316R mutant displays both extremes, having the most decreased polymerization rate and nucleotide binding most similar to wild type. Given that the active site residues are intact, this result suggests that either

another step is present in the polymerization mechanism that occurs between the ground-state binding of nucleotide in the active site and catalysis, the rate of phosphodiester bond formation is now rate limiting, or both.

Substitution of Glu316 with Arginine Disrupts the Hydrophobic Hinge. Computer modeling and molecular dynamics simulations of the Arg316 mutant show that the nucleotide binding pocket remains unaltered in the mutant as compared to the wild-type polymerase. This is reflected in the $K_{d(dNTP)}$ values, which are essentially identical (Table 5). The model shows that Coulomb repulsion between Arg316 and Arg182 in the mutant causes the charged side chains to move far apart, which in turn pushes them into the nearby hydrophobic hinge region (Figure S2). This causes both Tyr265 and Tyr266 to move out of their wild-type positions. Interestingly, the distance between Arg316 and Tyr266 is maintained throughout the fully equilibrated 5 ns simulation. Furthermore, the side chain of Arg316 lies in a semiopen position on the surface of the structure; the backbone position of Arg316 aligns with the backbone of Glu316 in the ternary (dNTP bound; 1bpy) structure, but the guanidinium headgroup aligns close to where the Glu316 glutamate carboxylate group is located in the binary (dNTP free; 1bpx) structure. This, along with the alterations in Tyr265 and Tyr266, could indicate that in the Arg316 mutant the fingers domain may be in an intermediate conformational state, being neither fully open nor fully closed relative to the palm domain and active site. This position allows for proper binding of dNTP in the nucleotide binding pocket, but suggests that other more subtle movements may be required to fully realize the complete chemical reaction.

The modeling of Arg316 pol beta suggests that there exists a relationship between the triad in the C-terminal domain and the hydrophobic hinge (Figure S2). The interaction between Arg182 and Glu316, which is located adjacent to the hydrophobic hinge, has been suggested to have a stabilizing effect on the open conformation of the hinge.[16] The open conformation is also supported by Tyr265,[17] which acts as a molecular doorstop helping the hinge stay open. As seen from the computer modeling, energy minimization, and the molecular dynamics simulations of the Arg316 mutant, the interaction between residues 182 and 316 is lost completely. The side chains have moved apart by 3.5 Å (2.9 Å in 1bpx wild type to 6.4 Å in the Arg316 model; Figure 7). This drastic separation, coupled with the similar nucleotide binding pocket volume and near-identical $K_{d(dNTP)}$ values, suggests that, although the polymerase does bind nucleotide, it cannot carry out the chemical reaction step. This disconnect between Arg182 and Arg316 could be disrupting the fingers domain movement, which could result in a polymerase that is no longer able to detect when nucleotide is bound in the active site and would cause a dramatic reduction in polymerase activity.

■ ASSOCIATED CONTENT

Ⓢ Supporting Information. Sequences of DNA oligonucleotide primers used for site-directed mutagenesis, circular dichroism spectra of the truncated mutants, and plots of distances between selected residues versus simulation time. This material is available free of charge via the Internet at http://pubs.acs.org.

■ AUTHOR INFORMATION

Corresponding Author
joann.sweasy@yale.edu

■ ACKNOWLEDGMENT

We thank K. Donigan for the donation of her wild-type pol beta protein and A. Nemec and K. Donigan for helpful discussions during this work.

■ REFERENCES

(1) Lindahl, T. *Nature* **1993**, *362*, 709–715.
(2) Prasad, R.; Beard, W. A.; Strauss, P. R.; Wilson, S. H. *J. Biol. Chem.* **1998**, *273*, 15623–15270.
(3) Pavlov, Y. I.; Maki, S.; Maki, H.; Kunkel, T. A. *BMC Biol.* **2004**, *2*, 11.
(4) Chou, K.-M.; Cheng, Y.-C. *Nature* **2002**, *415*, 655–659.
(5) Starcevic, D.; Dalal, S.; Sweasy, J. B. *Cell Cycle* **2004**, *3*, 998–1001.
(6) Venkatesan, R. N.; Bielas, J. H.; Loeb, L. A. *DNA Repair* **2006**, *5*, 294–302.
(7) (a) Plug, A. W.; Clairmont, C. A.; Sapi, E.; Ashley, T.; Sweasy, J. B. *Proc. Natl. Acad. Sci. U.S.A.* **1997**, *94*, 1327–1331. (b) Kidane, D.; Jonason, A. S.; Gorton, T. S.; Mihaylov, I.; Pan, J.; Keeney, S.; deRooij, D. G.; Ashely, T.; Keh, A.; Liu, Y.; Banerjee, U.; Zelterman, D.; Sweasy, J. B. *EMBO J.* **2010**, *29*, 410–423.
(8) Loeb, L. A.; Loeb, K. R.; Anderson, J. P. *Proc. Natl. Acad. Sci. U.S. A.* **2003**, *100*, 776–781.
(9) Murphy, D. L.; Kosa, J.; Jaeger, J.; Sweasy, J. B. *Biochemistry* **2008**, *47*, 8048–8057.
(10) Johnson, K. A. *Annu. Rev. Biochem.* **1993**, *62*, 685–713.
(11) Dalal, S.; Chikova, A.; Jaeger, J.; Sweasy, J. B. *Nucleic Acids Res.* **2008**, *36*, 411–422.
(12) DeLano, W. L. *The PyMOL Molecular Graphics System*; DeLano Scientific LLC: San Carlos, CA, 2006; http://www.pymol.org.
(13) Kalé, R. S.; Bhandarkar, M.; Brunner, R.; Gursoy, A.; Krawetz, N.; Phillips, J.; Shinozaki, A.; Varadarajan, A.; Schulten, K. *J. Comput. Phys.* **1999**, *151*, 283–312.
(14) Yamtich, J.; Starcevic, D.; Lauper, J.; Smith, E.; Shi, I.; Rangarajan, S.; Jaeger, J.; Sweasy, J. B. *Biochemistry* **2010**, *49*, 2326–2334.
(15) Lin, P.; Pedersen, L. C.; Batra, V. K.; Beard, W. A.; Wilson, S. H.; Pedersen, L. G. *Proc. Natl. Acad. Sci. U.S.A.* **2006**, *103*, 13294–13299.
(16) Pelletier, H.; Sawaya, M. R.; Wolfe, W.; Wilson, S. H.; Kraut, J. *Biochemistry* **1996**, *35*, 12742–12761.
(17) Shah, A. M.; Maitra, M.; Sweasy, J. B. *Biochemistry* **2003**, *42*, 10709–10717.